Title

A Glutamatergic Hypothalamomedullary Circuit Mediates Thermogenesis, but Not Heat Conservation, during Stress-Induced Hyperthermia.

Journal

Current biology : CB, 28(14)

ISSN

0960-9822

Authors

Machado, Natalia LS
Abbott, Stephen BG
Resch, Jon M
et al.

Publication Date

2018-07-01

DOI

10.1016/j.cub.2018.05.064

Peer reviewed

Published in final edited form as:

Curr Biol. 2018 July 23; 28(14): 2291–2301.e5. doi:10.1016/j.cub.2018.05.064.

A glutamatergic hypothalamomedullary circuit mediates thermogenesis but not heat conservation during stress-induced hyperthermia

Natalia L. S. Machado[1,2], **Stephen B.G. Abbott**[1,3], **Jon Resch**[4], **Lin Zhu**[1], **Elda Arrigoni**[1], **Bradford Lowell**[4], **Patrick M. Fuller**[1], **Marco A. P. Fontes**[2], and **Clifford B. Saper**[1,5,*]

[1.] Department of Neurology, Beth Israel-Deaconess Medical Center and Harvard Medical School, Blackfan circle, Boston 02215 USA

[2.] Department of Department of Physiology and Biophysics, Federal University of Minas Gerais, Antonio Carlos Ave., Belo Horizonte 31270-901 Brazil

[3.] Department of Pharmacology, University of Virginia, Jefferson Park Ave., Charlottesville 22908 USA

[4.] Division of Endocrinology, Diabetes, and Metabolism, Department of Medicine, Beth Israel Deaconess Medical Center, Harvard Medical School, Blackfan circle, Boston 02215 USA

Summary

Stress elicits a variety of autonomic responses, including hyperthermia (stress fever) in humans and animals. In this present study, we investigated the circuit basis for thermogenesis and heat conservation during this response. We first demonstrated the glutamatergic identity of the dorsal hypothalamic area (DHA^{Vglut2}) neurons that innervate the raphe pallidus nucleus (RPa) to regulate core temperature (Tc) and mediate stress-induced hyperthermia. Then, using chemogenetic and optogenetic methods to manipulate this hypothalamomedullary circuit, we found that activation of DHA^{Vglut2} neurons potently drove an increase in Tc, but surprisingly stress-induced hyperthermia was only reduced by about one-third when they were inhibited. Further investigation showed that DHA^{Vglut2} neurons activate brown adipose tissue (BAT), but do not cause vasoconstriction, instead allowing reflex tail artery vasodilation as a response to BATinduced hyperthermia. Retrograde rabies virus tracing revealed projections from DHA^{Vglut2} neurons to RPa^{Vglut3}, but not to RPa^{GABA} neurons and identified a set of inputs to $DHA^{Vglut2} \rightarrow$ RPa neurons that are likely to mediate BAT activation. The dissociation of the DHA^{Vglut2} thermogenic pathway from the

[*]Correspondence: csaper@bidmc.harvard.edu, Dept. of Neurology, Beth Israel Deaconess Medical Center, 330 Brookline Avenue, Boston, MA 02215.

[5.]Lead Contact

Author contributions: Study concept and design: N.L.S.M., S.B.G.A., M.A.P.F. and C.B.S.; Data acquisition and analysis: N.L.S.M., S.B.G.A., J.R., T.P.L., L.V., B.L. and P.M.F.; Drafting the manuscript and figures: N.L.S.M. and C.B.S.

Declaration of Interests: The authors declare no competing interests.

thermoregulatory vasoconstriction (heat conserving) pathway, may explain stress flushing (skin vasodilation, but a feeling of being too hot) during stressful times.

Introduction

Stress was initially defined as a psychological state that increased sympathetic activity [1] and later corticosteroid secretion [2] to prepare the body to face adversity, i.e., a “fight or flight”responses [1]. It is now understood to be marked by a suite of autonomic, endocrine and behavioral responses that are critical for mammals confronting aversive conditions in nature.

Under diverse stress paradigms (such as air jet, restraint, social defeat, novel cage, cage switch, handling and others) animals show patterns of autonomic response [3–5] that are similar to humans under psychological stress [6, 7]. Among these responses induced by stress is psychogenic fever or, more precisely, “stress-induced hyperthermia” [5], an elevation of core body temperature (Tc) generally without motor (shivering) response [7]. However, humans undergoing stress-induced hyperthermia often blush and feel warm.

By contrast, fever in response to an inflammatory stimulus or cooling typically involves both activation of brown adipose tissue (BAT) and constriction of cutaneous blood flow to conserve heat [8, 9]. Humans under cold conditions or during a fever are typically peripherally vasoconstricted and feel cold.

The region of the dorsomedial hypothalamus plays a critical role in adaptive increases in Tc by inducing thermogenesis [10, 8, 11] and vasoconstriction through an excitatory influence on the activity of cutaneous vasoconstriction (CVC) neurons [9]. In rodents, this thermoregulatory region includes both the dorsomedial hypothalamic nucleus (DMH) as well as the adjacent dorsal hypothalamic area (DHA) [12]. In rats the DHA contains a cluster of neurons which show cFos expression during stress or lipopolysaccharide challenge [13] and which have heavy projections to the raphe pallidus in the medulla (RPa) [13, 14]. Neurons in RPa mediate elevations in Tc by providing the necessary excitation to populations of spinal neurons that drive BAT and shivering thermogenesis, as well as tail artery vasoconstriction in rodents [15, 16]. Interestingly, Zhao et al., 2017 showed that activation of both cold responsive glutamatergic neurons (i.e, express the vesicular glutamate transporter 2,Vglut2), and GABAergic neurons in the DHA/DMH region causes elevation of Tc [17], but the chemical phenotype of the DHA → RPa neurons and their target cell types in the RPa remained undetermined.

In this study we identified the RPa-projecting, stress-activated DHA neurons as glutamatergic. We then used chemogenetic inhibtion and activation of these neurons to study their role in stress-induced hyperthermia. Finally, we used transneuronal rabies tracing to identify the phenotype of the RPa cells that the DHA^{Vglut2} neurons contact, and some of their inputs. These results indicate that the DHA^{Vglut2} neurons that project to the RPa provide a unique circuit for activating thermogenesis, but permitting reflex vasodilation, as occurs in humans with flushing during stress.

Results

Identification of RPa projecting-DHA neurons activated during stress

To identify the phenotype of DMH/DHA neurons projecting to RPa, we used 4 *Vgat-IRES-cre x L10-GFP* and 7 *Vglut2-IRES-cre x L10-GFP* reporter mice injected with retrograde tracer (CTb) in the RPa. We identified large numbers of glutamatergic DHA neurons labeled with CTb (79.05%), but virtually no GABAergic neurons in the DHA (0.03%) were found projecting to RPa (Figure 1A). The bulk of these doubly labeled neurons were located in the DHA along and just dorsal to the border of the dorsomedial hypothalamic nucleus at the level where the mammillothalamic tract rises above the dorsal edge of the third ventricle (Figures 1A and B). To determine whether these neurons also play a role in stress responses, we subjected 4 of the *Vglut2-IRES-cre-GFP* reporter mice injected with CTb in the RPa to our cage exchange stress protocol for two hours. In this protocol, a male mouse is moved to a new cage that was previously occupied by another male mouse [6]. In mice, we find a consistent increase in Tc over the next two hours to a maximum of 2.8°C ± 0.1 SEM, n=6 (Figures 2E and H). We then compared the expression of cFos protein in the DHA region in the 4 stressed mice with 3 similar mice that were maintained in their home cages and not handled. We observed that stress caused 39 ± 6% of Vglut2/CTb neurons to express cFos, whereas only 13 ± 2% of Vglut2/CTb neurons expressed cFos in the control animals (n= 4,3 respectively; *p=0.016, t-test t=3.538 df=5) (Figure 1C).

DHA^{Vglut2} neurons regulate Tc, mediate stress-induced hyperthermia and fever due to lipopolysaccharide (LPS) injection.

We then examined the role of DHA^{Vglut2} neurons in regulating thermal responses and locomotor activity (LMA) associated with cage exchange stress. We injected AAV-DIO-hGlyR into the DHA bilaterally in *Vglut2-IRES-cre* transgenic mice or wild type mice (WT) as a control. The hGlyR is a human glycine receptor that was mutated by Lynagh and Lynch [18] to no longer respond to glycine but to be approximately 100 times as sensitive to the antiparasitic drug ivermectin (IVM) as the endogenous human channel. To enable genetic encoding of this construct we generated a cre-dependent version (DIO-hGlyR) and packaged it into an AAV (Figure 2A). We injected *Vglut2-IRES-cre* transgenic mice with AAV-DIO-hGlyR-mCherry or AAV-FLEX-mCherry (control group) in the DHA and with fluorescent CTb (F-CTB conjugated with AlexaFluor-488) into the RPa. Whole-cell recordings in brain slices were conducted from RPa-projecting DHA^{Vglut2} neurons. These neurons were double labeled for F-CTb (retrogradely labeled from the RPa) and for hGlyR-mCherry or just mCherry (control animals) (Figure 2J). As expected, IVM (50 nM) silenced action potential firing or hyperpolarized the resting membrane potential of the DHA^{Vglut2} neurons expressing hGlyR-mCherry in all the neurons tested (n = 6), including 4 RPa-projecting DHA^{Vglut2} neurons double labeled for hGlyR-mCherry and F-CTb. IVM induced hyperpolarization of DHA neurons expressing hGlyR-mCherry (−2.70 ± 0.71 mV; n = 4) In two neurons, IVM silenced the firing but the effect on the resting membrane potential could not be assessed because these neurons had high spontaneous firing prior to IVM application. IVM had no effects on the firing or the resting membrane potential of DHA^{Vglut2} neurons that only expressed mCherry (control group: n = 6 DHA mCherry(+), including 3 RPa-projecting DHA^{Vglut2} double labeled for mCherry and F-CTb)(Figure 2I).

We chose the hGlyR-IVM approach because IVM has a long half-life allowing us to inject the drug one day, and test the animals the next day, which prevents us having to handle the animals immediately before testing. IVM is also reversible, so the same animal can be tested before, during and after IVM for internal controls; and it has been used successfully in behavioral studies at the doses used in this study [19–21]. Vglut2-Cre mice expressing hGlyR in the DHA (baseline Tc 35.6 ± 0.2°C) that were treated with IVM, but not otherwise exposed to stress, showed an initial hypothermic response of 1.5°C ± 0.6 SEM lasting about 3–4 hours. By 4–5 hours, Tc was no longer statistically different from control groups. No changes in Tc or LMA were observed in control Vglut2-Cre mice that received injections of AAV-DIO-hGlyR and vehicle (baseline Tc 35.7 ± 0.17°C), Vglut2-Cre mice that received injections of AAV-FLEX-ChR2-mCherry and IVM (baseline Tc 35.4 ± 0.25°C), or WT mice (baseline Tc 35.6 ± 0.16°C) that received injections of AAV-DIO-hGlyR and IVM (Figures 2D and F). We interpreted the response to IVM in the AAV-DIO-hGlyR treated Vglut2-Cre mice as evidence that the DHA^{Vglut2} neurons contribute to baseline thermogenesis or heat conservation. However, because IVM has a half-life of 2–3 days [19], we suspected that the subsequent normalization was due to reflex compensation by other thermoregulatory systems after inhibiting DHA^{Vglut2} neurons (Figures 2D and F).

We used cFos immunostaining to show the long-lasting inhibitory effect of hGlyR-IVM on DHA^{Vglut2} neurons during our stress protocol. We observed that 24h after injection of IVM there was a large reduction of cFOS expression induced by our stress protocol in the DHA of *Vglut2-IRES-cre* mice that had received injections of AAV-DIO-hGlyR, compared with control *Vglut2-IRES-cre* mice that received vehicle 24h before experiencing the stress protocol (IVM showed 6 ± 1% cFOS+ /hGlyR VGLUT2 labeled neurons vs vehicle 40 ± 8% cFOS+ /hGlyR VGLUT2 cFos doubly labeled neurons in the DHA (p=0.01, t-test t=4.256 df=4, n=3 each group) (Figure 2C).

Next to test whether DHA^{Vglut2} neurons are necessary to induce stress-induced hyperthermia, we injected IVM or vehicle 24h before cage exchange-induced stress, in *Vglut2-IRES-cre* mice expressing hGlyR in DHA^{Vglut2} neurons. We used *Vglut2-IRES-cre* mice injected with AAV-FLEX-ChR-mCherry as the virus control or WT mice injected with AAV-DIO-hGlyR as the genotype control. We observed that IVM induced a decrease of stress-induced hyperthermia of about 30% (T_{max} = 2.7 ± 0.09°C after vehicle vs. 2.0 ± 0.1°C after IVM vs. 7 days after IVM 3.0 ± 0.16°C, n=11) in *Vglut2-IRES-cre* mice with hGlyR transduced bilaterally in the DHA. *Vglut2-IRES-cre* mice transduced bilaterally in the DHA with AAV-DIO-hGlyR had a significant reduction in the hyperthermic response 24h after IVM when compared with the same animals' responses induced by stress 24h after vehicle or 7 days after IVM injection, but no changes were observed in the locomotor activity responses to stress when comparing these groups ($F_{Tc\ (36,540)}$=1.918, *p=0.0013 and $F_{lma\ (72,394)}$=0.9, p>0.05 two-way ANOVA, followed by Bonferroni's post hoc test) (Figures 2E and G). We used IVM due its half-life of about 2–3 days in rodents, which minimize animal handling stress once IVM and/or vehicle injection were performed at least 24h before the stress protocol. To determine how long its effects would last, we performed our stress protocol 24h, 48h and 7 days after IVM injection (Figure 2B). We observed that IVM was able to attenuate hyperthermia induced by stress 24h hours and 48h after IVM when compared with the responses 24h after vehicle in *Vglut2-IRES-cre.* However, the inhibition

promoted by the hGlyR-IVM was no longer apparent after 7 days. hGlyR unilaterally injected (n=7) and controls (AAV-ChR injected and WT, n=6 each) had normal and similar responses to our stress protocol (3.0 ± 0.35°C vs. 2.6 ± 0.25°C vs. 2.9 ± 0.11°C; $F_{(6,56)}$=8.266 One-way ANOVA, followed by Bonferroni's post hoc test *p<0.05) (Figure 2h).

We also examined the role of DHA^{Vglut2} neurons in mediating fever due to lipopolysaccharide (LPS), a bacterial cell wall component. IVM was injected 24h before LPS in the same *Vglut2-IRES-cre* mice transduced bilaterally with AAV-DIO-hGlyR in the DHA that were tested previously in our stress protocol. The IVM treatment reduced the immediate peak in Tc that is due to the stress of handling and injecting the mice, again by about 30%. Both the first (approx. 1° C, 45 min after LPS injection) and second (about 1.5° C, 120–150 minutes after injection) peaks in fever following LPS were almost eliminated compared to LPS effects 24h after injection of vehicle or injection of IVM in control mice (injected with the AAV-FLEX-ChR-mCherry in the DHA), although the more prolonged, approx. 0.7° C increase in Tc beginning at about 2 hr after LPS was unaffected. (Figure S1). We confirmed that LPS injection promoted activation of DHA^{Vglut2} neurons using cFos immunostaining 4h after injection of LPS. We observed greater cFOS expression in the DHA^{Vglut2} neurons of *Vglut2-IRES-cre-GFP* mice treated with LPS when compared with *Vglut2-IRES-cre* mice treated with saline as controls (Figure S1). Thus, these early peaks of LPS fever are dependent upon the activity of DHA^{Vglut2} neurons, and the hGlyR-IVM strategy is effective at eliminating that response, but the hyperthermic response to cage exchange stress must also depend upon additional mechanisms.

Activation of DHA^{Vglut2} neurons induces BAT thermogenesis but does not cause tail vasoconstriction

To better characterize the physiological effects of activating DHA^{Vglut2} neurons, we compared body temperature and locomotor activity recorded in *Vglut2-IRES-cre* mice expressing AAV8-hSyn-DIO-hM3D(Gq)-mCherry bilaterally in the DHA after treatment with clozapine-N-oxide (CNO) with the same mice after saline injection (baseline of both groups 35.6 ± 0.2°C), and WT mice (baseline 35.8 ± 0.15°C) injected with AAV8-hSyn-DIO-hM3D(Gq)-mCherry after CNO, as controls. We observed that, similar to Tan et al., 2016 and Zhao et al., 2017, hM3Dq activation of DHA^{Vglut2} neurons induced hyperthermia of up to 2.5°C ± 0.2°C - lasting for approximately 4.5 hours compared to controls after saline (1.6 ± 0.18°C) ($F_{Tc\ (144,1228)}$=2.931, two-way ANOVA, followed by Bonferroni's post hoc test, *p<0.0001; Saline/CNO, n=7 and WT after CNO, n=6) (Figure 3A), while increases in LMA lasted approximately 1.5 hour after CNO injection, compared with responses after saline injection or with WT mice treated with AAV8-hSyn-DIO-hM3D(Gq)-mCherry and CNO ($F_{LMA\ (144,1240)}$=1.715, two-way ANOVA, followed by Bonferroni's post hoc test, *p<0.0001; Saline/CNO, n=7 and WT CNO, n=6) (Figure 3A). We also tested if activation of DHA^{Vglut2} neurons would potentiate the hyperthermia and hyperactivity induced by cage exchange stress. However, Tc and LMA responses evoked by CNO during stress were similar to those seen after saline (Figure S2). In other words, the responses were not additive during cage exchange stress, suggesting that the DHA^{Vglut2} response is already activated near its maximum during stress-induced hyperthermia.

To determine the role of DHA^{Vglut2} neurons in the regulation of BAT and tail blood flow during stress hyperthermia, we used thermal imaging of the mice while we performed our cage exchange stress protocol or induced activation of DHA^{Vglut2} neurons with hM3Dq and CNO. Both conditions were compared with responses after saline injection, using thermal images for analyses. Both psychological stress and direct activation of DHA^{Vglut2} neurons produced long-lasting increases in the interscapular BAT temperature of 1.0 ± 0.14°C, mean for 2 hours ($F_{(8,76)}$=3.39 two-way ANOVA, followed by Bonferroni's post hoc test *p<0.05; Saline/CNO, n=7 and stress, n=8) (Figure 3B and C). However, unlike stress hyperthermia, in which the tail temperature dropped, the DHA^{Vglut2} activation caused a delayed increase in tail temperature by 2.5 ± 0.6°C for 2 hours, indicative of increased tail blood flow, beginning at about 30 minutes and lasting for about 90 minutes after CNO injection ($F_{(8,76)}$=3.26 two-way ANOVA, followed by Bonferroni's post hoc test *p<0.05; Saline/CNO, n=7 and stress, n=8) (Figure 3b, c and Video S1). Activation of DHA^{Vglut2} neurons by CNO (131.7 ± 53 cFos+ after CNO vs. 19 ± 6 in the control animals after saline, n= 3,4 respectively; *p=0.008, t-test t=2.50 df=5) (Figure 3D) also caused an increase in the number of neurons expressing cFos in the dorsolateral preoptic area (116 ± 29 cFos+ after CNO and 24 ± 8 in the control animals, n= 3,4 respectively; *p=0.01, t-test t=3.50 df=5); a similar magnitude of cFos expression was found in neurons in the RPa, but it did not reach statistical significance (80 ± 34 cFos+ after CNO vs. 23 ± 3 in the control animals after saline, n= 3,4 respectively p=0.09, t-test t=2.016 df=5) (Figure S3).

Optogenetic inhibition of DHA^{Vglut2}—>RPa reduces stress-induced hyperthermia

We next used photoinhibition of the synaptic terminals of DHA^{Vglut2} neurons in the RPa to test to what extent the RPa projection from DHA^{Vglut2} neurons is responsible for stress fever. We used mice injected with an AAV causing Cre-dependent expression of ArchT-GFP, a light-responsive proton pump that results in hyperpolarization of neurons for inhibitory optogenetic manipulation, and control mice injected with an AAV coding for Cre-dependent expression of GFP, in the DHA of *Vglut2-IRES-cre* mice. We used freely behaving mice at 22°C and compared the Tc of experimental mice (baseline 36.3 ± 0.3°C) with the Tc of control mice expressing only GFP in DHA^{Vglut2} neurons (baseline 36.2 ± 0.5°C) (Figure 4B). In mice in which AAV-FLEX-ArchT-GFP but not mice with the control vector injected bilaterally into the DHA, inhibiting the terminal field in the RPa with orange laser light for 15 min caused a reduction of baseline Tc of 0.79 ± 0.5°C.

We next tested whether inhibition of DHA^{Vglut2} synaptic terminals in the RPa was sufficient to reduce stress-induced hyperthermia using the same pattern of photoinhibition. We found that DHA^{Vglut2} synaptic terminal photoinhibition reduced the stress-induced hyperthermia by 0.4 ± 0.1°C SEM compared to hyperthermic responses before optogenetic inhibition (although the light from the optical fiber probably did not cover the entire length of the RPa, Figure 4D). We also tested the stress responses the day after the photoinhibition as a control for any damage to the RPa that might be caused by the laser stimulation; here we found that the magnitude of the hyperthermic response during stress was 0.7 ± 0.1°C SEM greater than that during the laser photoinhibition (Figure 4C). Baseline Tc prior to cage exchange of the groups tested for the stress protocol did not differ (35.6 ± 0.6C before STIM vs. 35.8 ± 0.6C STIM vs. 35.2 ± 0.5C after STIM).

Afferents to RPa-projecting DHA^{Vglut2} neurons

Using transneuronal rabies mapping, we examined the regions potentially sending projections to RPa-projecting DHA^{Vglut2} neurons and the phenotype of RPa neurons that putatively receive DHA^{Vgltu2} inputs. G-deficient rabies virus was injected in the RPa and AAVs expressing the G and TVA proteins were transduced into DHA^{Vglut2} neurons. This caused replication competent rabies-GFP to be expressed in the DHA^{Vglut2} neurons, confirming their projections to the RPa (Figure 5C). Substantial numbers of neurons that provided putative afferents to the DHA^{Vglut2} → RPa circuit were also labeled in these experiments in the median preoptic nucleus (MnPO), dorsolateral preoptic area (DLPO), parastrial nucleus (PS), suprachiasmatic nucleus (Sch), paraventricular hypothalamic nucleus (PVH), lateral hypothalamic area (LH), dorsomedial hypothalamic nucleus (DMH) and lateral parabrachial nucleus (LPBN) (Figure 5G-N). A few rabies-GFP neurons were also found in the supraoptic nucleus, nucleus accumbens, paraventricular thalamic nucleus, zona incerta, periaqueductal grey matter, median raphe nucleus and possibly local neurons in the DHA. We used a traditional tracer method (cholera toxin B subunit, CTb) and confirmed that the cell groups with substantial putative inputs to the DHA^{Vglut2} neurons do send axons to the DHA (Figure S4), thus eliminating that they were secondary afferents (i.e., labeled transneuronally from one of the other primary afferents to the DHA).

In addition, we injected Cre-dependent AAVs for G and TVA proteins, as well as the rabies –GFP virus, into the RPa in *Vglut3-IRES-Cre* mice to identify putative monosynaptic inputs to RPa^{Vglut3} neurons. These experiments demonstrated robust expression of rabies-GFP in DHA neurons (4 mice) (Figure 5A); by contrast when we injected *Vgat-IRES-Cre* mice with the same combination, there were very few rabies-GFP labeled neurons in the DHA (2 mice) (Figure 5B). Although the transneuronal efficiency of rabies may vary among cell types, the DMH^{Vglut2} neurons that target the RPa appear to end primarily on Vglut3 rather than Vgat neurons in the RPa. Furthermore, these results provide insight into the afferents to the DHA^{Vglut2} →RPa neurons which include key sites involved in thermoregulation and emotion that can be explored in future experiments to define the role of these regions in mediating stress responses.

Discussion

Our study demonstrates that the DHA neurons that project to the RPa express Vglut2 and are therefore glutamatergic neurons selectively activated by stress. We then showed that targeted chemogenetic inhibition of DHA^{Vglut2} cell bodies or optogenetic inhibition of the DHA^{Vglut2} → RPa terminals strongly decreased baseline body temperature and attenuated stress-induced hyperthermia by about one-third. Activation of the DHA^{Vglut2} neurons with the hM3Dq receptor caused hyperthermia of at least the magnitude and duration of stress-induced hyperthermia, which was accompanied by tail artery vasodilatation, indicating that during a stress response, the DHA^{Vglut2} neurons account for the activation of BAT, but not the cutaneous vasoconstriction. Finally, by using rabies virus retrograde tracing, we found that DHA^{Vglut2} neurons project to the Vglut3, but not the Vgat-expressing neurons in the RPa, and identified a set of inputs to DHA^{Vglut2} → RPa neurons, at least one of which is likely to mediate the BAT thermogenesis during stress-induced hyperthermia.

Although the stimulation of the DHA^{Vglut2} neurons could replicate a hyperthermic response with the amplitude and duration of stress-induced hyperthermia, the inhibition of the DHA^{Vglut2} neurons was only able to reduce the stress fever response by about one-third. A previous study by Kataoka et al., 2014 also found blunting of stress-induced hyperthermia after injecting muscimol (agonist $GABA_A$) in the DMH region, but did not determine the cell types that were affected. Our inhibtion was restricted to Vglut2 neurons, but it is likely that our injections of viral vectors into the DHA did not transduce all of the neurons that contribute to this pathway, so the inhibition we observed should be viewed as a lower bound for the contribution of the DHA^{Vglut2} neurons to stressinduced hyperthermia. On the other hand, activation of DHA^{Vglut2} neurons with hM3Dq/CNO was only able to activate BAT thermogenesis, and did not cause tail vasoconstriction (in fact, there was reflex vasodilation of the tail artery as Tc climbed). As activation of BAT and CVC is ordinarily coordinated during stressful conditions [22] our results suggest that the primary action of the DHA^{Vglut2} neurons is on BAT, and that vasoconstriction is caused by a separate pathway. Thus even complete inhibition of the DHA^{Vglut2} neurons would not be expected to extinguish stress-induced hyperthermia completely.

Interestingly, during the first few hours after LPS injection, inhibition of the DHA^{Vglut2} neurons was able to block LPS fever. Administration of LPS models an inflammatory fever, and is thought to involve both BAT thermogenesis as well as arterial vasoconstriction [9, 23], but apparently the BAT activation is particulary critical in the early phases of this fever model, and depends on the DHA^{Vglut2} neurons. Similarly, warm-responsive neurons in the ventral part of the median preoptic nucleus projecting to the region containing the DHA inhibit BAT thermogenesis but not tail vasodilation responses [24]. The median preoptic neurons that express EP3 prostaglandin receptors are also necessary for fever responses to intracerebral prostaglandin E2 or systemic LPS [25], and we were able to ablate the early fever response to i.p. LPS by inhibiting the DHA^{Vglut2} neurons with our hGlyR receptor. These findings are consistent with the possibility that the DHA^{Vglut2} neurons are a synaptic intermediary between the ventral median preoptic nucleus to the RPA^{Vglut3} neurons, which is critical for fever production. On the other hand, a second pathway must regulate the heat conservation, which is not mediated via the DHA^{Vglut2} pathway during stress-induced hyperthermia. One candidate for the vasoconstrictive pathway would be the cold responsive GABAergic (Vgatexpressing) neurons in the DMH that also drive increases in Tc [17]. Alternatively, other preoptic neurons, involved in regulating warm responses but not fever, may alter Tc by means of direct projections to the RPa, as various non-specific electrical, chemical or optogenetic stimulation of the median preoptic or dorsolateral preoptic cell groups drive changes in vasomotor responses as well as BAT [26, 16, 27, 28].

Vasoconstrictor responses are thought to be mediated by Vglut3 neurons in the RPa [29, 30]. However, here we show that DHA^{Vglut2} neurons access the Vglut3-expressing neurons but not Vgat-expressing neurons in the RPa. This result would suggest that there may be two populations of RPa^{Vglut3} neurons, one of which receives DHA^{Vglut2} input and only drives BAT, whereas the other group receives no DHA^{Vglut2} input and is responsible for tail artery vasoconstriction. GABAergic neurons in the DMH region were recently reported also to promote an increase in Tc and LMA [17]. We found that DHA^{Vgat} neurons sent very sparse projections to RPa and do not show cFos expression in response to stress, but we did not test

the functionality of these RPa-projecting DHA^{Vgat} neurons. In addition, the injections used by Zhao and colleagues in the DMH were much larger than ours (200 nl vs 15–20 nl), and included a much larger region (apparently including the DHA as well as most of the DMH, cf. their Fig. 3B with our fig. 4d). Additional studies will be needed to investigate the circuitry involving GABAergic neurons in the DMH region regulating thermal and locomotion changes.

The use of rabies virus retrograde transsynaptic tracing also entails some limitations. Although the rabies virus is often claimed to transfer between neurons only across synapses, and it is certainly possible that this is the case, this is a very difficult hypothesis to prove [31–33]. Our own data indicating the presence of DHA retrograde labeling when the rabies virus is propagated from RPa^{Vglut3} neurons but not RPa^{Vgat} neurons may potentially provide evidence for transsynaptic selectivity of rabies virus racing. We tried to confirm in slice preparations that activation of DHA^{Vglut2} terminals causes EPSPs on RPa^{Vglut3} but not RPa^{GABA} neurons. However, obtaining recordings of the raphe pallidus neurons is exceedingly difficult in brain slices prepared from adult mice, largely due to the density of myelinated fibers that hamper visualization of the neurons. For this reason, in vitro electrophysiological studies of raphe pallidus neurons have generally been conducted in neonatal mice. Unfortunately, because it takes 4–6 weeks after injection of the AAV before stable expression is established, it is not possible to apply these methods in neonatal animals. We rely on our anatomical data and the physiological evidence that the activation of DMH neuron terminals in the RPa increases BAT temperature [3] and inhibition of DHA^{Vglut2} terminals in the RPa promotes a decrease in Tc and reduction of stress-induced hyperthermia, to suggest the role of an excitatory DHA^{Vglut2} → RPa^{Vglut3} pathway in the regulation of thermogenesis.

The pattern of inputs observed to the DHA^{Vglut2} → RPa neurons reveals inputs from key thermoregulatory regions such as the MnPO that contain both warm-responsive neurons [26, 24] and cold-responsive neurons [27], and the LPB that contains coldactivated Foxp2+ neurons [34]. Both of these regions may provide good starting points for future work. In particular, it will be necessary to use optogenetic stimulation or similar methods to confirm the functional connectivity of these regions observed using the rabies tracing.

In conclusion, the present work shows that a DHA^{Vglut2} → RPa^{Vglut3} pathway activates BAT thermogenesis to cause stress-induced hyperthermia, but is not responsible for the heat-conserving vasoconstriction during this response. Activation of this independent heat-producing pathway may drive the flushing phenomenon (skin vasodilation associated to a feeling of being too hot) during certain emotional states such as embarrassment, an association that is not seen during typical thermoregulatory processes.

STAR METHODS

CONTACT FOR REAGENT AND RESOURCE SHARING

Further information and requests should be directed to and will be fulfilled by the Lead Contact, Clifford Saper (csaper@bidmc.harvard.edu)

EXPERIMENTAL MODEL AND SUBJECT DETAILS

Animals—All animal care and experimental procedures were approved by the Beth Israel Deaconess Medical Center Institutional Animal Care and Use Committee. We used male and female heterozygous *Vglut2-IRES-cre* and *Vgat-IRES-Cre* [35] and *Vglut3-IRES-cre [36],* some of which were mated to Cre-dependent GFP reporter mice (Vglut2-IRES-Cre;R26-loxSTOPlox-L10-GFP and Vgat-IRES-Cre;R26-loxSTOPlox-L10-GFP) [34]. Mouse lines were generated by L. Vong and B.B. Lowell (BIDMC, Harvard University), back-crossed to Jackson Labs C57BL6, and underwent genotyping before experiments. The age of mice at the time of experimentation ranged between 12–30 weeks and littermates of same sex were randomly assigned to experimental groups. Mice were individually housed in standard plastic cages with standard corn cob bedding with nesting materials on a 12 h light: 12 h dark cycle at ambient temperatures ranging between 22 ± 2°C. Mouse chow (Teklad F6 Rodent Diet 8664) and water were provided *ad libitum.*

METHOD DETAILS

Neural tracers and Viral Vectors

Cholera toxin subunit B (CTb) (1% diluted in saline, List Biological Labs) was microinjected for retrograde anatomical experiments in the volume of 6–9nL.

AAV8-FLEX-TVA-mCherry (titre 1.1 3 1012 genomes copies per ml) from the University of North Carolina vector core (UNC). Injections were made using the volume of 30– 45nL.

AAV8-FLEX-RG(titre 1.4 3 1012 genomes copies per ml) from the Stanford Gene Vector and Virus Core Injections were made using the volume of 30–45nL.

SADDG-EGFP (EnvA pseudotyped) rabies (titre 107 genomes copies per ml) from the Salk Institute Gene Transfer, Targeting, and Therapeutics Core. Injections were made using a volume of 100nL.

AAV8-hSyn-DIO-hM3D(Gq)- mCherry produced at the University of North Carolina virus core was used in the volume of 15–20nL

AAV8-DIO-ChR2 (H134R)-mCherry-WPRE (ChR) generously provided by K. Deisseroth (Stanford University) and the AAVs produced at the University of North Carolina vector core. We used the same volume of hGlyR virus injections: 45–60nL.

AAV8-CAG-FLEX-ArchT-GFP) that co-expresses the Archaerhodopsin TP009 T (ArchT) in a Cre dependent manner. This virus vector was procured from the University of North Carolina vector core (UNC). Injections were made using the volume of 30– 90nL.

AAV8-CAG-FLEX-GFP) that expresses the GFP in a Cre dependent manner. This virus vector was procured from the University of North Carolina vector core (UNC). Injections were made using the volume of 30–90nL.

hGlyR vector construction - Novel cell specific inhibitor

We used a modified human alpha-1 glycine receptor gene, previously tested in vitro [18], in which A288G and F207A mutations were induced to render the channel almost 100 times more sensitive to the antiparasitic IVM, but insensitive to glycine. The construct was placed within a FLEX cassette and packaged into AAV, serotype 10. Injections of the AAV-DIO-hGlyR were made using the volume of 45–60nL.

In vitro electrophysiology

We injected 9 Vglut2-IRES-cre mice (5 females and 4 males) with AAV-DIO-hGlyR-mCherry or AAV-FLEX-mCherry and after 3 weeks we injected CTb conjugated with fluorescence Alexa-488 (F-CTb). Following about 10 days after F-CTb injection, we euthanized the mice for slice recordings. Brain slices are prepared using the same methods as described in our recent work (Ferrari et al., 2018 J. Neurosci). Briefly, mice were deeply anesthetized with 5% isoflurane via inhalation and transcardially perfused with ice-cold artificial cerebrospinal fluid (ACSF; W-methyl-D-glucamine, NMDG-based solution). NMDG-based ACSF solution) contains (in mM): 100 NMDG, 2.5 KCl, 1.24 NaH_2PO_4, 30 $NaHCO_3$, 25 glucose, 20 HEPES, 2 thiourea, 5 Na-L-ascorbate, 3 Na-pyruvate, 0.5 $CaCl_2$, 10 $MgSO_4$ (pH 7.3 with HCl when carbogenated with 95% O_2 and 5% CO_2). We quickly removed the mouse brains block off the brainstem containing the injection site of F-CTB in RPa, to be fixed overnight in formalin and we sectioned the forebrain in coronal slices (250 mm thick) in ice-cold NMDG-based ACSF using a vibrating microtome (VT1200S, Leica, Bannockburn, IL, USA). Brain slices are recorded in normal ACSF containing (in mM): 120 NaCl, 2.5 KCl, 1.3 $MgCl_2$, 10 glucose, 26 $NaHCO_3$, 1.24 NaH_2PO_4, 4 $CaCl_2$, 2 thiourea, 1 Na-L-ascorbate, 3 Na-pyruvate (pH 7.4 when carbogenated with 95% O_2 and 5% CO_2, 310–320 mOsm). Recordings were conducted using a combination of fluorescence and infrared differential interference contrast (IR-DIC) video microscopy. We recorded in whole-cell configuration using a Multiclamp 700B amplifier (Molecular Devices, Foster City, CA, USA), a Digidata 1322A interface, and Clampex 9.0 software (Molecular Devices). We recorded in current-clamp mode at resting membrane potential if the cells were spontaneously active. If the recorded DHA neurons were silent at resting membrane potential, we inject a depolarizing holding currents or 5 ms depolarizing pulses to produce action potential firing. We recorded using a we used a K-gluconate-based pipette solution containing (in mM): 120 K-Gluconate, 10 KCl, 3 $MgCl_2$, 10 HEPES, 2.5 K-ATP, 0.5 Na-GTP (pH 7.2 adjusted with KOH; 280 mOsm). We added 0.5% biocytin in the pipette solution to mark the recorded neurons. Immediately following the *in vitro* recordings, the recorded slices were fixed overnight in formalin and then processed to fluorescently label the recorded neurons. We incubated the recorded slices overnight in streptavidin-conjugated Alexa-405 (1: 500; Invitrogen) to label the recorded neurons filled with biocytin. We verified the location of the recorded neurons in the DHA expressing hGlyR-mCherry or mCherry and the presence of F-CTB under fluorescence microscopy. We cut the formalin-fixed block of brainstem containing the RPa into 40 mm sections on a freezing microtome and examined the sections under fluorescence microscopy to validate the location of the injected F-CTB in the RPa.

Surgery

All surgeries were performed in sterile conditions. Mice were anesthetized with the mix of ketamine/xylazine (100 and 10 mg/kg, respectively, IP) with additional doses of 10% of the initial dose throughout surgery to eliminate the withdrawal reflex. Stereotaxic microinjections were made into the DHA (coordinates: AP = −1.85 mm, L = 0.3, DV = −4.45 mm from Bragma) and RPa (coordinates: AP = −2.2 mm, L = 0.0, DV = −5.5 mm from Lambda), and the optical fiber implant coordinates were 300–500 μm dorsal to RPa. Mice were implanted with a radiotelemetry temperature sensor (TA-F10, DSI) in the intra peritoneal space via laparotomy. Meloxicam treatment, for analgesia, was administered prior to surgery then again 24hrs later. Mice were allowed to recover at least 10 days prior to experimentation. Following recovery, mice used for experiments showed no signs of discomfort and gained weight normally.

Intraperitoneal injection and specific ligands

Ivermectin (IVM) (Ivomec, Merial) was used as the specific ligand to hGlyR (5mg/Kg) diluted in propylene glycol. Propylene glycol was used as control (1 μl/g). IVM is known to have a long half-life (2–3 days) in mice, so recordings were done on the second day after injection, when the animals had recovered from the acute effects of handling and drug injection.

Clozapine-N-oxide (CNO) was used at the dose of 0.3mg/kg (sigma, catalog #34233– 69-7) as specific ligand to AAV8-hSyn-DIO-hM3D(Gq)- mCherry.

Lipopolysaccharides from Escherichia coli 0111:B4 (LPS), (sigma catalog #L2630) 20μg/Kg.

Core temperature recordings

Tc was recorded using the radiotelemetry DSI system. The signal was sent from the telemetry probes previously implanted to receivers and converted using the PhysioTel HD and PhysioTel (DSI) hardware which provides the mean of Tc every 5 minutes. The optogenetic experiments were performed using Spike software (CED), and DSI probes were calibrated by placing the probe in a bath water at 30 and 35°C and using a radiotelemetry data logger to record the time course change of the mean temperature every minute, the gain and offset of the probe determined by linear regression between the voltage recorded at each set-point via the radiotelemetry data logger (0.125°C accuracy) [26]. All animals had at least 48hours of acclimation in the recording chamber before baseline was recorded.

Thermal imaging

Thermal imaging was performed in Vglut2-IRES-cre mice during the light phase using an infrared camera (FLIR E4) [26, 34]. After at least 4 weeks from the AAV8-hSyn-DIO-hM3D(Gq)- mCherry injection, the back, neck and head of the mouse was shaved under low dose of ketamine/xylazine. Following 5 days recovering from anesthesia effects and 48h for habituation, mice received injections of CNO or saline (7 males), or exchange cage stress was performed (8 males). Thermal images from pictures and videos recorded the time course changes in BAT temperature (TBAT) and tail temperature (Ttail). Both videos and

images were used to determine TBAT (using a mean of the temperature between the right and left scapula) and Ttail (using tree different points from the body to the most distal region of the tail) FLIR tools software was used for all analysis.

Stress protocol

Singly housed male mice were switched to an empty cage that was previously occupied by a single male (exchange cage stress), then after 2 hours under stress the mice were switched back to their previous home cage. Stress protocols were always performed following at least 48 hours of acclimation, between 12:00pm and 2:00pm EST and food and water were provided during the protocols *ad libitum.*

Photoinhibition

Photoinhibition was performed using a yellow-orange light laser (593 nm; LaserGlow) controlled by Spike 8.01 software and patterns consisted of 10 stimuli of 60 seconds delivered at 8–12 mV with a 30 seconds interval between every stimulus. For the stress protocol 4 stimulus of 60 seconds delivered at 8–12 mV with a 30 seconds interval between every stimulus were provided before switching the mice to a dirty cage. The pattern and duration of photoinhibition was determined empirically based on preliminary experiments to produce maximal physiological effects without causing tissue damage. During these initial experiments, we observed tissue damage using the parameter of continuous photostimulation for 30 minutes.

Monosynaptic rabies virus tracing

AAV-FLEX-TVA and AAV-FLEX-RG were injected unilaterally in the DHA of 5 *Vglut2-IRES-Cre* mice or in the RPa of 4 *Vglut3-IRES-Cre* and 5 *Vgat-IRES-Cre* mice. Following four weeks to permit appropriate expression of helper viruses G-deleted, rabies-GFP vector was injected into the RPa of all mice.

Perfusion and brain sectioning

After performing the experimental protocols or 7–10 days after Cholera toxin subunit B (CTb) injections mice were deeply anesthetized with chloral hydrate (1.5% BW i.p. 7% solution) and transcardially perfused with 30ml phosphate buffer saline and then 30ml 10% pH neutral formalin (Fischer). Brains were extracted and post fixed overnight in 10% formalin and then stored in 20% sucrose until sectioned using a freezing microtome (40 μm coronal sections into 3 series). Following sectioning tissue was stored at 4°C in PBS containing the preservative so dium azide until processed for histology.

Injection sites

In order to confirm the injection sites, one series of the tissue was mounted and cover slipped with hard-set mounting media (Vectashield) for native fluoresce GFP (ArchT) and mCherry (ChR). The AAV8-hSyn-DIO-hM3D(Gq)-mCherry or AAV-Flex-hGlyR-mCherry mCherry were labeled using immunochemistry, then the tissue was mounted and cover slipped with Permamount (Fischer Chemical). We used a mouse brain atlas (Franklin and Paxinos, 2007) to determine coordinates for injection sites. Only animals with the

histological confirmation of the region targeted were used for analyses. We used a heatmap showing overlapping of the hM3Dq-mCherry+ injection sites of every mouse used in this experiment. To construct the heatmap we converted the photomicrography of the injection site into a binary one, applied a Gaussian filter to remove remaining noise and stacked them together using Matlab.

Immunohistochemistry

All sections were processed free floating and conducted at room temperature. For CTb immunofluorescence the sections of the tissue were rinsed, and incubated in a blocking solution of 10% horse serum, then rinsed and incubated with primary antibody overnight. Sections were then rinsed and incubated with secondary antibody for 2 hours for double labeled experiments. Experiments using triple labeled cells after the primary antibody rinsing, sections incubated with a biotinylated secondary antibody for 2 hours, then rinsed and incubated with Streptavidin Cy5 conjugate antibody for 2 hours. Sections were rinsed and mounted onto glass slides, air dried and dehydrated through a series of graded alcohols and xylenes and covered with DPX mounting media. For the 3,3-diaminobenzidine immunohistochemistry sections were rinsed and incubated in 1 % hydrogen peroxide 2.5% triton X100, 1% NHS in PBS for 10 minutes then incubated with primary antibody overnight. After rinsing, sections incubated with a biotinylated secondary antibody for 120 minutes, rinsed and incubated in ABC solution (1:500, Vector) for 60 minutes. Sections were then rinsed and incubated DAB (Sigma) plus 0.02% H_2O_2. The sections were stained brown with DAB only or black by adding 0.05% cobalt chloride and 0.01% nickel ammonium sulfate to the DAB solutions. For dual DAB staining, the sections were rinsed overnight and the process repeated. Sections were finally rinsed, mounted, Nissl counter-stained.

Antibodies

mCherry protein was detected using a cross-reacting rabbit polyclonal anti-DSRED antibody (1:5,000, Clontech, catalog #14088015). cFOS was detected using rabbit polyclonal antiserum against residues 4–17 from human c-Fos (AB5, 1:20,000; Oncogene Sciences, catalog #484). For DAB and Streptavidin immunochemistry, we used the secondary antibody: donkey anti-rabbit biotinylated-IgG (1:1000, Jackson ImmunnoResearch Laboratories, catalog #711065152). For fluorescence histochemistry, we used the goat anti-CTb (1:10000, list biologicals, catalog #703) then secondary antibody Cy3-tagged anti-rabbit-IgG (1:500, Jackson ImmunnoResearch Laboratories, catalog #705165003) was used to visualize red fluorescence or Streptavidin Cy5 conjugate antibody was used to visualize purple fluorescence (1:500, Invitrogen, catalog #SA1011). No staining was seen when the primary DSRED or CTb antibodies were used on tissue from uninjected mice, or when secondary antibodies were tested without the primary antibodies.

QUANTIFICATION AND STATISTICAL ANALYSIS

Quantitative analyses of histology

To determine the number of all retrograde neurons and FOS-imunnoreactive cells (cFOS) in the DHA/DMH, we counted neuron bodies and nuclei at the level where the

mammillothalamic tract (mt) rises the dorsal edge of the third ventricle. We placed the counting box dorsal to VMH and ventral to the mt. and used the mt as the lateral border to the box. To count the number of FOS-imunnoreactive cells in the DHA, the counting box was placed at the dorsal border of the DMH and ventral to mt using the mt as limit for the lateral border.

Statistical analysis

Statistical analysis were performed using GraphPad Prism v7 (GraphPad Software). Significant differences were determined using a paired t-test, unpaired t-test, or repeated measures one-way and two-way ANOVA followed by Bonferroni's post-hoc test. Mann-Whitney and Friedman tests were used when data failed to the D'agostino-Pearson normality test. Data are presented as mean ± SEM. The statistical test used, statistical significance and number of animal subjects per group are reported in results and figure legends, data were considered to be statistically significant when $p<0.05$. No blinding was used, however all animals used in our experiments were sacrificed after completion of the study and viral expression, injection sites and optical fiber placement were verified as criteria for assignment of animals in experimental and control groups.

Supplementary Material

Refer to Web version on PubMed Central for supplementary material.

Acknowledgments:

We thank Joseph Lynch for generously providing the DNA cassette containing the mutated human α1 GlyR subunit. Supported by U.S. NIH Grants NS085477and NS072337. N.L.S.M. and M.A.P.F were supported by CNPq (National Council for Scientific and Technological Development / Brazil - Grants 200881/2014–0 and PQ30600/2013–0), CAPES (Coordination for the Improvement of Higher Education Personnel) S.B.G.A. was supported by an early career fellowship from the National Health and Medical Research Council of Australia (Grant GNT1052674) L.Z. and E.A. were supported by U.S. NIH Grant 1R01NS091126.

References

1. Cannon W (1929). Bodily changes in pain, hunger, fear and rage, Second Edition, (Appleton and Co.).
2. Selye H (1955). Stress and disease. Int Rec Med Gen Pract Clin 168, 277–287.14381095
3. Vinkers CH , Groenink L , van Bogaert MJ , Westphal KG , Kalkman CJ , van Oorschot R , Oosting RS , Olivier B , and Korte SM (2009). Stress-induced hyperthermia and infection-induced fever: two of a kind? Physiol Behav 98, 37–43.19375439
4. Vinkers CH , de Jong NM , Kalkman CJ , Westphal KG , van Oorschot R , Olivier B , Korte SM , and Groenink L (2009). Stress-induced hyperthermia is reduced by rapid-acting anxiolytic drugs independent of injection stress in rats. Pharmacol Biochem Behav 93, 413–418.19520106
5. Kataoka N , Hioki H , Kaneko T , and Nakamura K (2014). Psychological stress activates a dorsomedial hypothalamus-medullary raphe circuit driving brown adipose tissue thermogenesis and hyperthermia. Cell Metab 20, 346–358.24981837
6. Oka T , Oka K , and Hori T (2001). Mechanisms and mediators of psychological stress-induced rise in core temperature. Psychosom Med 63, 476–486.11382276
7. Oka T (2015). Psychogenic fever: how psychological stress affects body temperature in the clinical population. Temperature (Austin) 2, 368–378.27227051
8. Dimicco JA , and Zaretsky DV (2007). The dorsomedial hypothalamus: a new player in thermoregulation. Am J Physiol Regul Integr Comp Physiol 292, R47–63.16959861

9. Rathner JA , Madden CJ , and Morrison SF (2008). Central pathway for spontaneous and prostaglandin E2-evoked cutaneous vasoconstriction. Am J Physiol Regul Integr Comp Physiol 295, R343–354.18463193
10. Zaretskaia MV , Zaretsky DV , Shekhar A , and DiMicco JA (2002). Chemical stimulation of the dorsomedial hypothalamus evokes non-shivering thermogenesis in anesthetized rats. Brain Res 928, 113–125.11844478
11. Cao WH , Fan W , and Morrison SF (2004). Medullary pathways mediating specific sympathetic responses to activation of dorsomedial hypothalamus. Neuroscience 126, 229–240.15145088
12. Fontes MA , Xavier CH , de Menezes RC , and Dimicco JA (2011). The dorsomedial hypothalamus and the central pathways involved in the cardiovascular response to emotional stress. Neuroscience 184, 64–74.21435377
13. Sarkar S , Zaretskaia MV , Zaretsky DV , Moreno M , and DiMicco JA (2007). Stress- and lipopolysaccharide-induced c-fos expression and nNOS in hypothalamic neurons projecting to medullary raphe in rats: a triple immunofluorescent labeling study. Eur J Neurosci 26, 2228–2238.17927775
14. Yoshida K , Li X , Cano G , Lazarus M , and Saper CB (2009). Parallel preoptic pathways for thermoregulation. J Neurosci 29, 11954–11964.19776281
15. Cao WH , and Morrison SF (2006). Glutamate receptors in the raphe pallidus mediate brown adipose tissue thermogenesis evoked by activation of dorsomedial hypothalamic neurons. Neuropharmacology 51, 426–437.16733059
16. Ootsuka Y , and McAllen RM (2006). Comparison between two rat sympathetic pathways activated in cold defense. Am J Physiol Regul Integr Comp Physiol 291, R589–595.16601257
17. Zhao ZD , Yang WZ , Gao C , Fu X , Zhang W , Zhou Q , Chen W , Ni X , Lin JK , Yang J , et al. (2017). A hypothalamic circuit that controls body temperature. Proc Natl Acad Sci U S A.
18. Lynagh T , and Lynch JW (2010). An improved ivermectin-activated chloride channel receptor for inhibiting electrical activity in defined neuronal populations. J Biol Chem 285, 14890–14897.20308070
19. Lerchner W , Xiao C , Nashmi R , Slimko EM , van Trigt L , Lester HA , and Anderson DJ (2007). Reversible silencing of neuronal excitability in behaving mice by a genetically targeted, ivermectin-gated Cl- channel. Neuron 54, 35–49.17408576
20. Oishi Y , Williams RH , Agostinelli L , Arrigoni E , Fuller PM , Mochizuki T , Saper CB , and Scammell TE (2013). Role of the medial prefrontal cortex in cataplexy. J Neurosci 33, 9743–9751.23739971
21. Todd WD , Fenselau H , Wang JL , Zhang R , Machado NL , Venner A , Broadhurst RY , Kaur S , Lynagh T , Olson DP , et al. (2018). A hypothalamic circuit for the circadian control of aggression. Nat Neurosci 21, 717–724.29632359
22. Mohammed M , Ootsuka Y , and Blessing W (2014). Brown adipose tissue thermogenesis contributes to emotional hyperthermia in a resident rat suddenly confronted with an intruder rat. Am J Physiol Regul Integr Comp Physiol 306, R394–400.24452545
23. Saper CB , Romanovsky AA , and Scammell TE (2012). Neural circuitry engaged by prostaglandins during the sickness syndrome. Nat Neurosci 15, 1088–1095.22837039
24. Tan CL , Cooke EK , Leib DE , Lin YC , Daly GE , Zimmerman CA , and Knight ZA (2016). Warm-Sensitive Neurons that Control Body Temperature. Cell.
25. Lazarus M , Yoshida K , Coppari R , Bass CE , Mochizuki T , Lowell BB , and Saper CB (2007). EP3 prostaglandin receptors in the median preoptic nucleus are critical for fever responses. Nat Neurosci 10, 1131–1133.17676060
26. Ootsuka Y , and Tanaka M (2015). Control of cutaneous blood flow by central nervous system. Temperature (Austin) 2, 392–405.27227053
27. Tanaka M , McKinley MJ , and McAllen RM (2011). Preoptic-raphe connections for thermoregulatory vasomotor control. J Neurosci 31, 5078–5088.21451045
28. Abbott SBG , and Saper CB (2017). Median preoptic glutamatergic neurons promote thermoregulatory heat loss and water consumption in mice. J Physiol 595, 6569–6583.28786483
29. Nakamura K , Matsumura K , Hubschle T , Nakamura Y , Hioki H , Fujiyama F , Boldogkoi Z , Konig M , Thiel HJ , Gerstberger R , et al. (2004). Identification of sympathetic premotor neurons

in medullary raphe regions mediating fever and other thermoregulatory functions. J Neurosci 24, 5370–5380.15190110

30. Lkhagvasuren B , Nakamura Y , Oka T , Sudo N , and Nakamura K (2011). Social defeat stress induces hyperthermia through activation of thermoregulatory sympathetic premotor neurons in the medullary raphe region. Eur J Neurosci 34, 1442–1452.21978215
31. Krashes MJ , Shah BP , Madara JC , Olson DP , Strochlic DE , Garfield AS , Vong L , Pei H , Watabe-Uchida M , Uchida N , et al. (2014). An excitatory paraventricular nucleus to AgRP neuron circuit that drives hunger. Nature 507, 238–242.24487620
32. Weissbourd B , Ren J , DeLoach KE , Guenthner CJ , Miyamichi K , and Luo L (2014). Presynaptic partners of dorsal raphe serotonergic and GABAergic neurons. Neuron 83, 645–662.25102560
33. Callaway EM , and Luo L (2015). Monosynaptic Circuit Tracing with Glycoprotein-Deleted Rabies Viruses. J Neurosci 35, 8979–8985.26085623
34. Geerling JC , Kim M , Mahoney CE , Abbott SB , Agostinelli LJ , Garfield AS , Krashes MJ , Lowell BB , and Scammell TE (2016). Genetic identity of thermosensory relay neurons in the lateral parabrachial nucleus. Am J Physiol Regul Integr Comp Physiol 310, R41–54.26491097
35. Vong L , Ye C , Yang Z , Choi B , Chua S , and Lowell BB (2011). Leptin action on GABAergic neurons prevents obesity and reduces inhibitory tone to POMC neurons. Neuron 71, 142–154.21745644
36. Cheng L , Duan B , Huang T , Zhang Y , Chen Y , Britz O , Garcia-Campmany L , Ren X , Vong L , Lowell BB , et al. (2017). Identification of spinal circuits involved in touch-evoked dynamic mechanical pain. Nat Neurosci.

Highlights)

- DHA glutamatergic neurons that innervate RPa are selectively activated by stress
- DHA^{Vglut2} neurons activation promotes BAT thermogenesis, but not vasoconstriction
- Inhibition of DHA^{Vglut2} neurons or their terminals in the RPa reduces stress fever
- DHA^{Vglut2} neurons project to the RPa^{Vglut3}, but do not innervate RPa^{VGAT} neurons

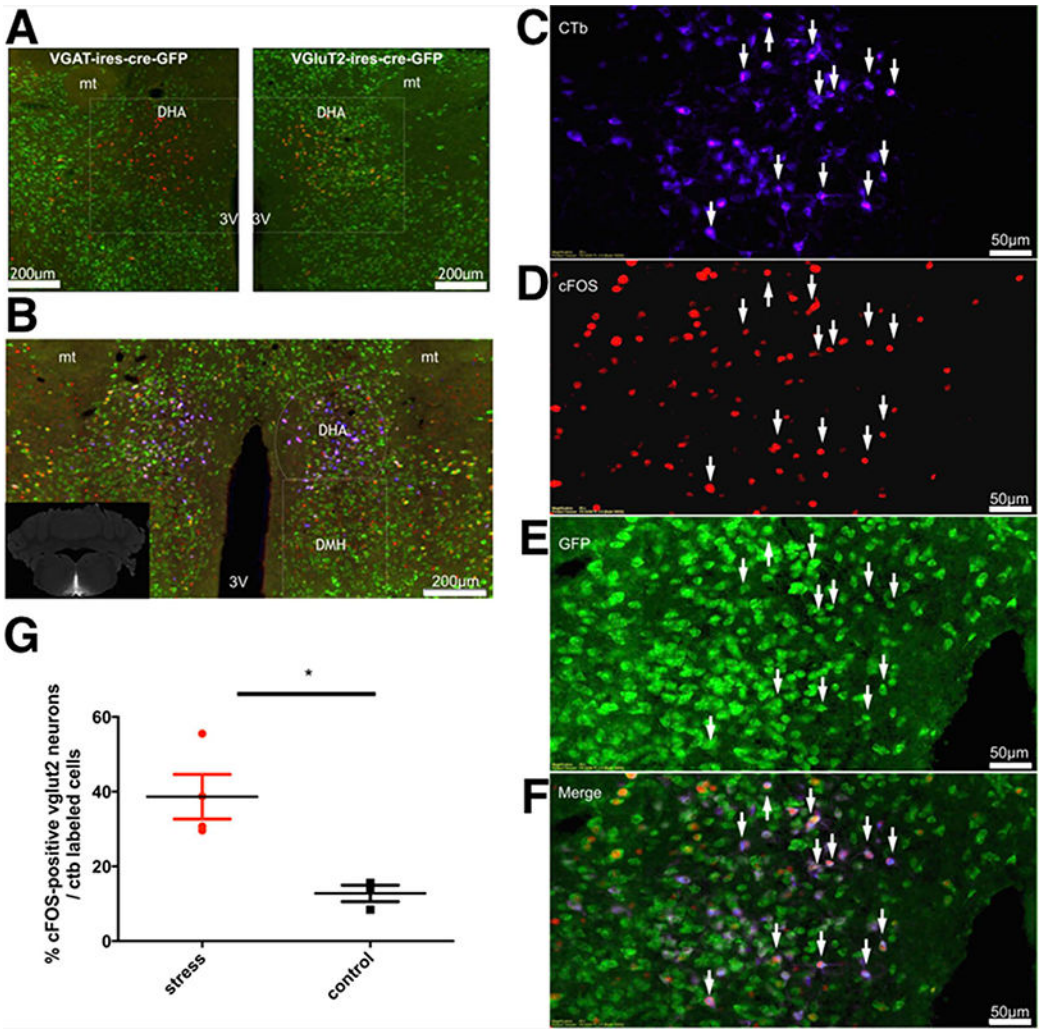

Figure 1. Identification of RPa projecting-DHA neurons activated during stress.

(A) Neurons in the dorsal hypothalamic area (DHA) were retrogradely labeled (red) by an injection of Cholera Toxin subunit b (CTb) in the medullary raphe pallidus (RPa) of *Vgat-IRES-cre-GFP* mice, n=4 and *Vglut2-IRES-cre-GFP* mice, n=7. Note that the retrograde label is highly colocalized with Vglut2 (yellow color in right panel). (B) Many of the Vglut2 neurons (green) that project to the RPa (blue; see inset for injection site) also contain c-fos (red). These neurons appear purple in this triple color scheme. Panels C-F show the left side of panel D at higher magnification. (G) Approximately 39 ± 6 % of the neurons retrogradely labeled from the RPa also containd cFOS and VGLUT2 in animals subjected to cage exchange stress, but only about 13 ± 2% in non-stressed control animals. *Statistical difference between groups (stress, n=4 and control, n=3) (p=0.0166, t-test=3.538 df=5). Abbreviations: 3V, third ventricle; mt, mammillothalamic tract.

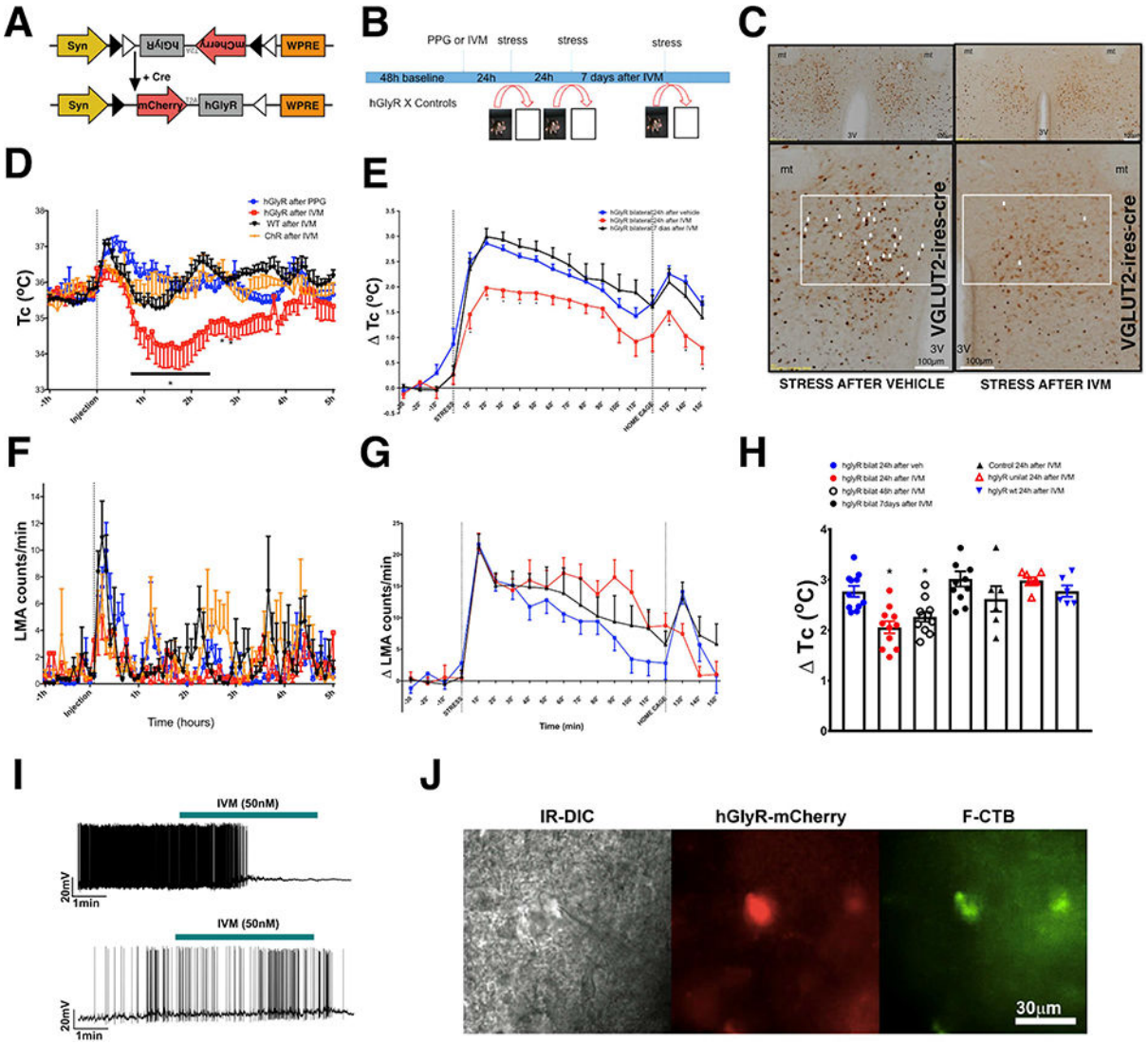

Figure 2. Inhibition of DHAVglut2+ neurons promotes hypothermia and reduces hyperthermia and cFOS expression induced by stress.

(A) Schematic figure of the DIO-hGlyR-T2A-mCherry construction, and its response to Cre recombinase. (B) Schematic figure of stress protocol. After recording baseline Tc for 48 hr, animals are given either IVM or vehicle (polypropylene glycol, PPG). Animals are then subjected to cage exchange stress at 24 hr, 48 hr, and 7 d after injection. (C) Reduction of stressinduced cFOS immunoreactivity 24h after IVM in mice exposed to psychological stress expressing hGlyR bilaterally in DHA Vlgut2 neurons. 40% ± 8 of neurons labeled for hGlyR-mCherry (brown) showed cFOS (black) expression during cage exchange stress after vehicle, but only 6.0 ± 1% after IVM (unpaired t-test, p=0.01 n=3 each group). (D) Tc (core temperature) and (F) LMA (locomotor activity) measurements in *Vglut2-IRES-cre* mice expressing hGlyR bilaterally in the DHA after i.p. injection of either vehicle or IVM (n=7) and in WT mice injected with the hGlyR or *Vglut2-IRES-cre* mice injected with AAV-ChR2, as controls after IVM (n=5 each). Mice in which the DHA Vglut2 neurons expressing hGlyR were inactivated by IVM injection showed a statistically significant hypothermia of

2° C ± 0.4 SEM for about 2–3 hours, but no statistically significant change in LMA. By 4–5 hrs after IVM, their Tc had returned to the same baseline as control animals $F_{Tc(interaction)\ (216,1342)}$=1.1254 $F_{tc(IVM)\ (3,1342)}$=81.14, two-way ANOVA followed by Bonferroni's post hoc test *p<0.05 and $F_{LMA(interaction)\ (213,1424)}$=1.171 $F_{lma(ivm)\ (3.1424)}$=1.613, two-way ANOVA followed by Bonferroni's post hoc test p>0.05 (e) Acutely inhibiting the DHA Vglut2 neurons ameliorates the stress-induced hyperthermia at 24 h, but not 7d after IVM injection. Graphs show changes in Tc after IVM or vehicle (2.7 ± 0.09°C after vehicle vs. 2.0 ± 0.1°C after IVM vs. 7 days after IVM 3.0 ± 0.16°C, n=11) (G) and LMA during psychological stress 24h and 7d after PPG or IVM injection (n=11). $F_{Tc\ (36,540)}$=1.918 two-way ANOVA followed by Bonferroni's post hoc test *p=0.0013 and $F_{lma\ (72,394)}$=0.9, p>0.05. (H) Greatest change in Tc induced by stress in mice expressing hGlyR bilaterally 24h after vehicle or 24h, 48h and 7 days after IVM (n=11) and in mice expressing hGlyR unilaterally or controls AAV-ChR and WT 24h after IVM (n=11, 7, 6 and 6 respectively) (h) $F_{(6,56)}$=8.266 One-way ANOVA, followed by Bonferroni's post hoc test *p<0.0001.(I) IVM silenced action potential firing of the RPa-projecting DHA^{Vglut2} neuron expressing hGlyR-mCherry. See also Figure S1. The top panel shows the current-clamp recording of a DHA neuron expressing hGlyR-mCherry and F-CTb in a slice preparation of Vglut2-IRES-cre mouse, IVM (50nM, green bar above traces) silences the action potential firing of a neuron. The bottom panel shows the currentclamp recording of a DHA neuron expressing mCherry and CTb in a slice preparation of a Vglut2-IRES-cre mouse (control), IVM (50nM, green bar above traces) has no effect on firing of control cells. (J) A DHA recorded neuron can be visualized under infrared (IR-DIC) and this same neuron colocolize hGlyR-mCherry (red) and F-CTb (green).

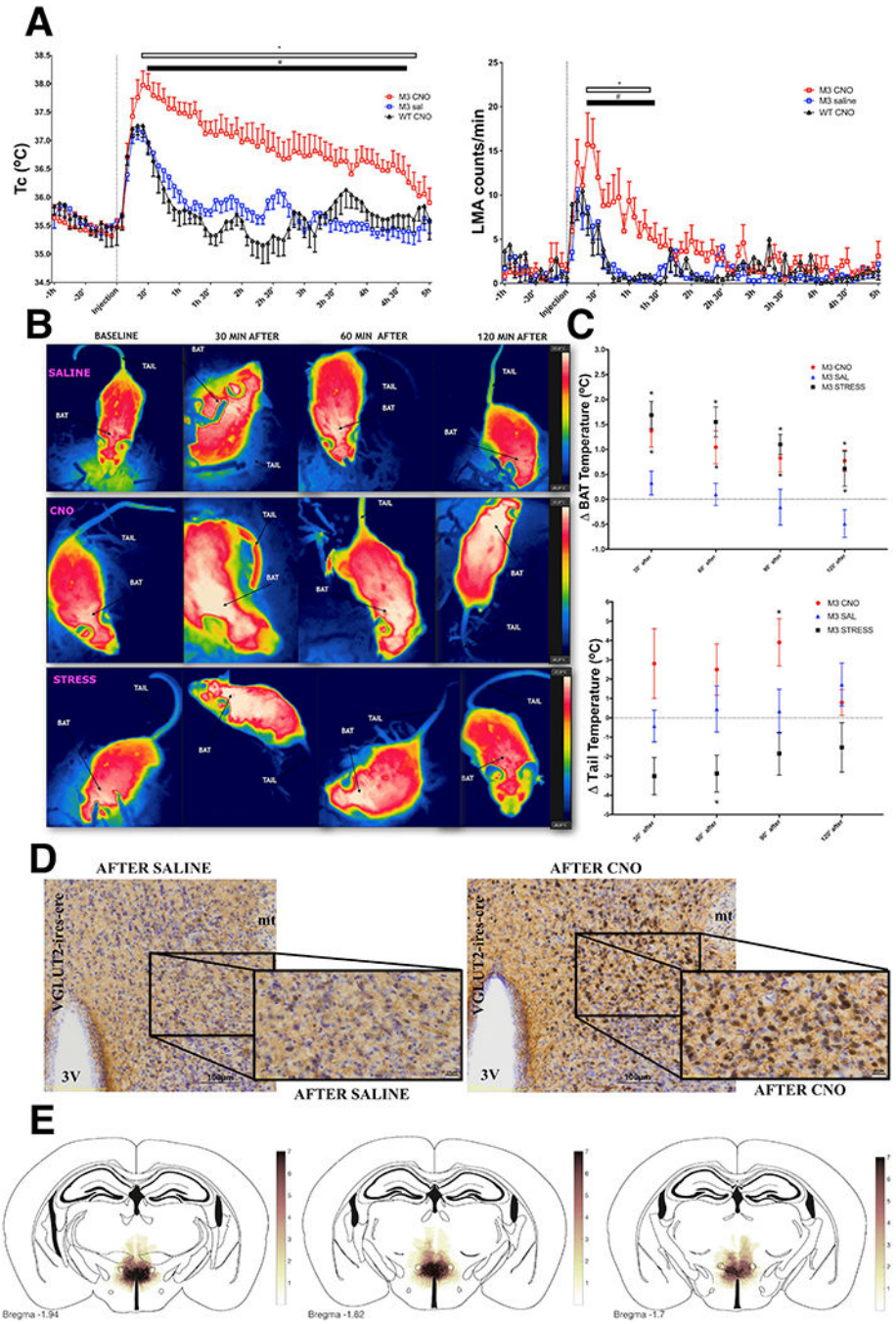

Figure 3. Activation of DHA$^{Vglut2+}$ neurons induces an increase in body temperature and locomotor activity.

(A) Activation of DHA^{Vglut2} neurons expressing the hM3Dq receptor (M3) by clozapine N-oxide (CNO, red) vs. saline caused a 1.5– 2.0°C elevation of Tc and a large increase in LMA; saline (n=7), CNO (0.3mg/kg) (n=7) and wild type mice after CNO (0.3mg/kg) (WT CNO, n=6) $F_{Tc\ (144,1228)}$=2.931, $F_{LMA\ (144,1240)}$=1.715, two-way ANOVA, followed by Bonferroni's post hoc test *p<0.0001 for M3 CNO compared with M3 saline; # p<0.0001 for M3 CNO compared with WT CNO. See also Figure S2. (B) Thermographic images showing temperature changes over the intrascapular brown adipose fat pad (BAT) and tail in

mice in which DHA^{Vglut2} neurons express hM3Dq (see also Video S1). The images across show baseline temperatures, then 30, 60 and 120 min after either an injection of saline (upper row, in which there is a small intial increase in BAT temperature corresponding with the fever of handling in panel a); or an injection of CNO (middle row, in which there is a strong increase in both BAT and tail temperature). By contrast, during cage exchange stress (lowest row), there is both activation of BAT and tail vasoconstriction, causing a lower tail temperature. (C)This paradoxical increase in both BAT and tail temperature in the animals treated with CNO (i.p.0.3mg/kg, n=7) compared to saline is shown quantitatively (n=7) $F_{(8,76)}$=3.26 two-way ANOVA, followed by Bonferroni's post hoc test *p<0.05. Psychological stress (n=8) by contrast induces an increase in BAT temperature similar to CNO $F_{(8,76)}$=3.39, along with tail cooling, similar to the response to cooling or LPS. (D)CNO induces massive activation of cFos (black nucleus) in DHA^{Vglut2} neurons that express hM3D(Gq)-mCherry (brown cytoplasm right) compared to injection of animals with saline (left), see also Figure S3. (E) A heatmap showing overlap of AAV-DIO-hM3Dq-mCherry injection sites in the DHA.

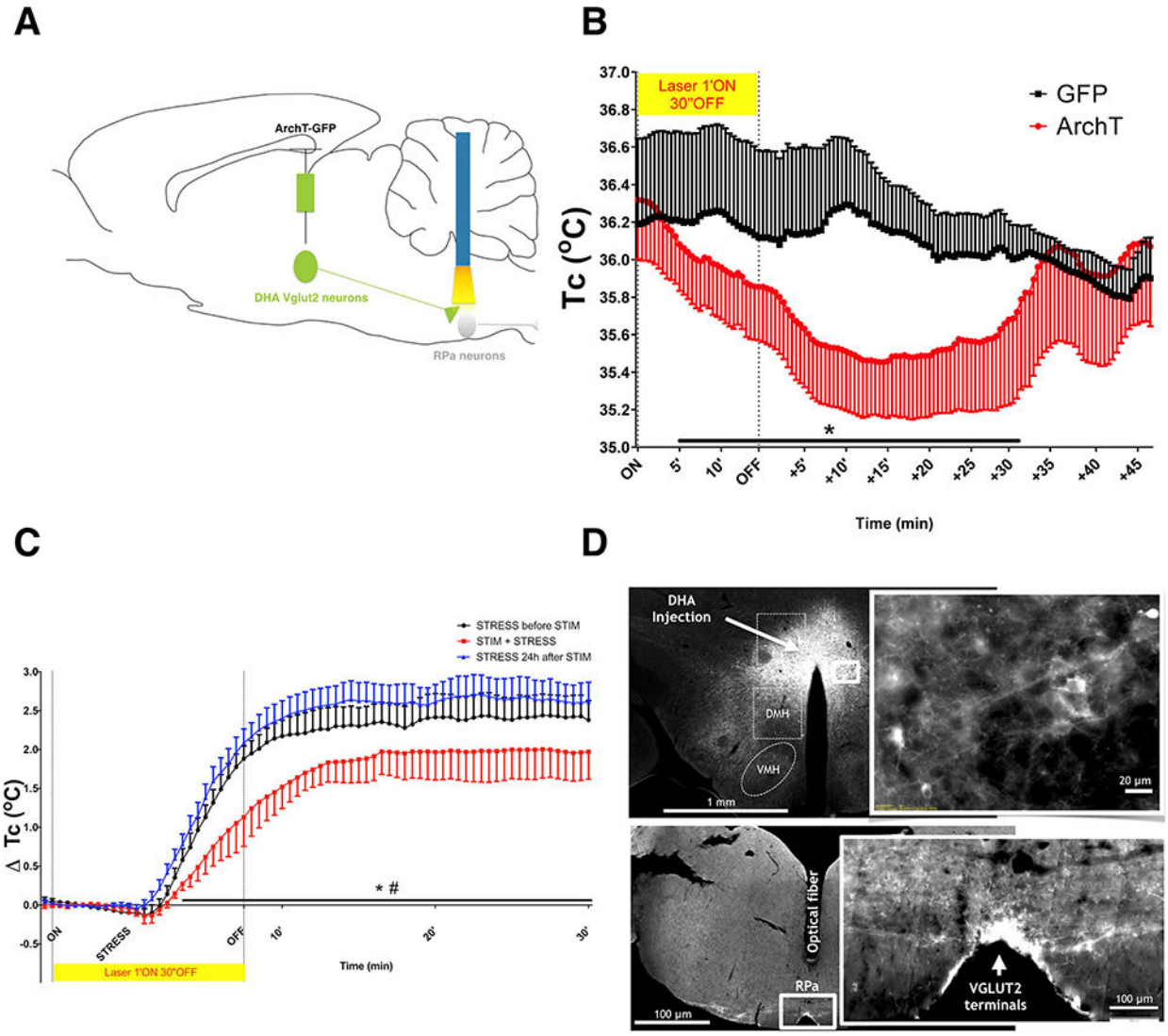

Figure 4. Optogenetic inhibition of DHA^{Vglut2} fibers in the RPa decreases body temperature and reduces stress-induced hyperthermia.

(A) A schematic figure of the protocol for inhibition of DHA VGLUT2+ fibers in the RPa using AAV-DIO-ArchT-GFP. (B) Core temperature measurement in *Vglut2-IRES-cre* mice injected in the DHA bilaterally with AAV-DIO-ArchT-GFP (n=5) or controls injected with GFP (n=6) during optogenetic inhibition of DHA^{Vglut2} terminals in the RPa (35.73 ± 0.02°C ArchT vs. 36.15 ± 0.008°C GFP controls during first 30 minutes after initiation of laser stimulation, Mann-Whitney test *p<0.0001). The laser inhibition causes an approximately 1°C fall in Tc at maximum which is about 10 min after the termination of the laser inhibition. (C) Core temperature measurement in *Vglut2-IRES-cre* mice injected in the DHA bilaterally with with AAV-DIO-ArchT-GFP (n=5) during the stress protocol before, during and after optogenetic inhibition of DHA^{Vglut2} terminals in the RPa (1.9 ± 0.01°C 24h before vs. 1.47 ± 0.009°C during vs 2.14 ± 0.01°C 24h after stimulation over the 30 minutes under cage exchange stress, Friedman test, # 24h before vs. during stimulation * 24h after vs. during stimulation p<0.0001). The stress causes an approximately 1.8°C increase in Tc

during the period of laser stimulation in the control animals, but only 1.0° C increase in the animals with ArchT terminals.(D) Representative fluorescence images of ArchT-GFP+ expression in DHA neurons in *Vglut2-IRES-cre* mice (upper left, low magnification, upper right, higher magnification of the area in the box) and in synaptic terminals in the RPa (lower left shows the level of the medulla and the track left by the optical fiber, lower right shows a high magnification view of the RPa).

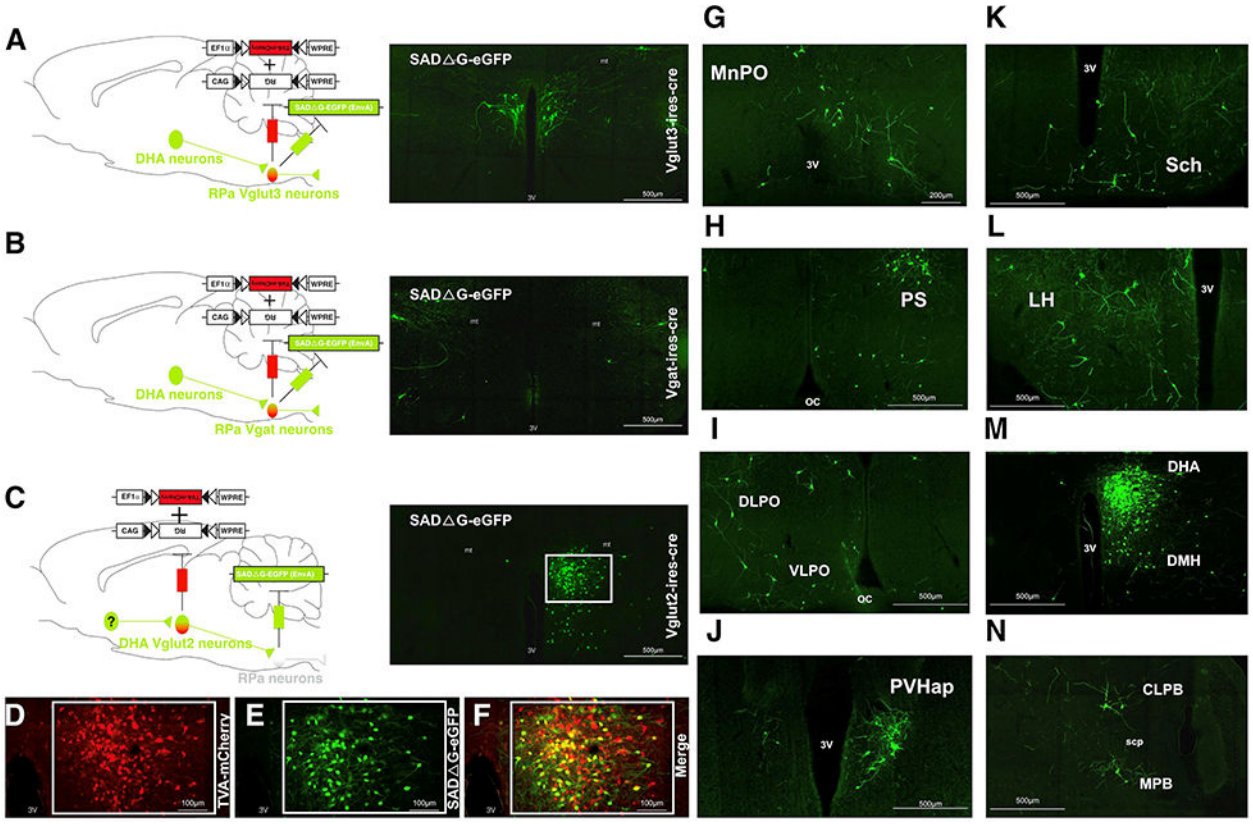

Figure 5. Mapping inputs to DHA^{Vglut2} --> RPa^{Vglut3} neurons using rabies virus.

(A) Schematic illustration of injecting the rabies virus plus Cre-dependent helper virus into the RPa in *Vglut3-Cre* mice (n=4). Retrogradely labeled (green) neurons were found in the DHA. (B) By contrast, after similar injections in *Vgat-Cre* mice (n=5), there was no retrograde labeling of DHA neurons, suggesting that DHA^{Vglut2} inputs selectively target Vglut3–5HT principal cells vs GABAergic interneurons in the RPa. (C) After injection of rabies virus in the RPa, but Cre-dependent helper virus only in the DHA of *Vglut2-Cre,* extensive retrograde virus was seen in the DHA. (D-F) Co-localization of the virus helper (TVA-mCherry) and virus labeled with eGFP is shown at higher magnificiation, n=5. (G-N) In the latter experiment, putative inputs to DHA^{Vglut2} --> RPa neurons were found from the: (G) median preoptic nucleus (MnPO), (H) parastrial nucleus (PS), (I) lateral preoptic areas (LPO), (J) paraventricular hypothalamic nucleus, (K) suprachiasmatic nucleus (Sch), (L) lateral hypothalamic area (LH), (M) dorsomedial hypothalamic nucleus (DMH), and (N) lateral and medial parabrachial nuclei (LPB and MPB respectively). See also Figure S4. Anatomic references: 3V, third ventricle; oc, optic chiasm; scp, superior cerebellar peduncle.